Available online at www.eccomasproceedia.org
Eccomas Proceedia COMPDYN (2025) 4610-4622

ECCOMAS
Proceedia

COMPDYN 2025
10th ECCOMAS Thematic Conference on
Computational Methods in Structural Dynamics and Earthquake Engineering
M. Papadrakakis, M. Fragiadakis (eds.)
Rhodes Island, Greece, 15-18 June 2025

EXPERIMENTAL-TO-ANALYTICAL MODELLING OF SSI FOR A SMALL-SCALE WIND TURBINE

Shahin Huseynli*, Ella E. Lee, Dimitris Karamitros, Raffaele De Risi, Matthew S. Dietz, and Flavia De Luca

[1] School of Civil, Aerospace and Design Engineering, University of Bristol, Bristol, United Kingdom
e-mail: {shahin.huseynli, zp21599, d.karamitros, raffaele.derisi, m.dietz, flavia.deluca}@bristol.ac.uk

Abstract

Soil-structure interaction (SSI) significantly affects the dynamic behaviour of monopile-supported offshore wind turbines, including the case of seismic loading. This study combines small-scale physical testing and analytical modelling to investigate these effects in a reduced-scale system representing a 2 MW turbine. Shaking table experiments were performed using a single-degree-of-freedom (SDOF) model embedded in a shear box filled with sand. Dynamic excitation was applied via white noise and scaled ground motions, with impact tests conducted before and after excitation to establish the natural frequency and damping. Results indicate a measurable reduction in natural frequency and increase in damping due to SSI, with these effects intensifying under higher input motion levels, where soil response becomes non-linear. These effects were also manifested in the bending strains recorded along the pile. More specifically, analytical modelling of inertial interaction based on a beam-on-elastic-foundation framework with elastic soil stiffness produced good agreement with experimental results under elastic conditions. However, at higher excitation levels, where the soil response became non-linear, the analytical model increasingly underestimated the experimentally measured bending response. This discrepancy arises primarily because the analytical model does not account for stiffness degradation associated with non-linear soil behaviour. These findings highlight the limitations of linear models and the value of integrating experimental, numerical, and analytical methods to inform future SSI-inclusive design approaches for offshore wind turbines.

Keywords: soil-structure interaction (SSI), wind turbines, monopile foundations, dynamic response, shaking table testing, Beam-on-Winkler foundation

ISSN:2623-3347
Peer-review under responsibility of the organizing committee of COMPDYN 2025.
doi: 10.7712/120125.12761.25582

1 INTRODUCTION

Offshore wind turbines supported by monopile foundations are particularly sensitive to soil-structure interaction (SSI) effects due to their slender proportions and significant heights. These structures often feature fundamental frequencies near those associated with rotor rotation and blade passing, making accurate dynamic characterisation essential for safe and effective design [1]. Small-scale experimental studies have consistently shown that the flexibility of soil support can significantly reduce the fundamental frequency compared to fixed-base assumptions, highlighting the need to incorporate SSI into dynamic analyses [e.g., 1, 2].

Numerous studies have employed experimental and numerical approaches to investigate SSI phenomena in offshore wind turbines. Bhattacharya and Adhikari [2] demonstrated experimentally how SSI significantly reduces turbine frequencies, while Lombardi et al. [1] further illustrated how cyclic loading affects stiffness and energy dissipation in soil-pile systems. Recent research has incorporated realistic combinations of operational and environmental loading. For example, shaking table tests with simultaneous wind and earthquake loads [3], as well as soil-water-structure interaction [4, 5], have provided deeper insight into SSI effects. Complementary models, from advanced finite element simulations to simplified spring-dashpot models, have enhanced the understanding of dynamic response and structural demand under extreme loading conditions, also highlighting the effects of soil liquefaction and higher-mode vibrations [6–8].

Despite these significant advances, important gaps remain. Current design guidelines recommend the use of simplified soil reaction models (e.g., *p-y* curves), which have not been rigorously validated for the case of loading scenarios encountered in offshore wind turbines [9]. Moreover, accurately scaling results from small-scale experimental models to full-scale turbine prototypes remains challenging, especially under complex operational loadings. While integrated studies linking experimental results to analytical predictions under realistic combined load conditions remain essential for bridging the gap between laboratory-scale insights and full-scale applications, the present study represents an initial step towards addressing this gap by combining small-scale testing and simplified analytical modelling.

Using shaking table experiments on a scaled single-degree-of-freedom (SDOF) model representing a 2 MW wind turbine founded on a monopile in granular soil, the research characterises the system's dynamic response under seismic excitations. The experimental investigation is complemented by an analytical approach based on available simplified analytical models, allowing comparisons with observed SSI behaviour, particularly in terms of natural frequency, damping, and pile bending under predominantly elastic conditions. The limitations of these simplified analytical models in capturing non-linear damping and stiffness degradation under stronger excitation are highlighted through these comparisons. The primary novelty of this work lies in the systematic integration of controlled laboratory testing with simplified analytical solutions, highlighting clear limitations of current design methodologies and informing future small- and full-scale testing campaigns.

2 EXPERIMENTAL SETUP

The experimental programme applies established scaling laws to replicate the seismic response of a full-scale 2 MW wind turbine [10] using a reduced 1-g shaking table model, while accommodating practical limitations of laboratory testing. The properties and dimensions of the prototype and model-scale monopiles are summarised in Table 1.

A key non-dimensional parameter governing dynamic similarity is the relative flexibility ratio, GL^4/EI, where G is the soil shear modulus, L is the pile length, E is the pile's Young's

modulus, and I is the second moment of area [11]. The relationship between scaling factors can be expressed as:

$$\lambda_{EI} = \lambda_L^4 \lambda_G = \lambda_L^{9/2} \tag{1}$$

Assuming $\lambda_G = \lambda_L^{1/2}$ for non-cemented sands, Equation (1) ensures that the model maintains consistent relative flexibility with the prototype. To preserve dynamic similarity, the natural frequency ratio between the model and prototype is used as a dynamic time scaling factor, defined in Equation (2):

$$\frac{\omega_m}{\omega_p} = \lambda_f = \lambda_L^{3/4} \tag{2}$$

where ω_m and ω_p are the natural frequencies of the model and prototype, respectively. Agreement between the calculated and theoretical ratios in Equation (2) supports the consistency of dynamic behaviour across scales.

	Length [m]	**Outer diameter [m]**	**Thickness [m]**	**Young's modulus [GPa]**	**Shear modulus [GPa]**	**Second moment of area [m^4]**
Prototype	15	3.5	0.05	210	80.8	0.8065
Model	0.41*	0.0255	0.001	70	26	5.785×10^{-9}

Table 1: Properties of prototype and model-scale monopile for a 2 MW wind turbine.

* The geometric scaling factor ($\lambda_L = 37$) corresponds directly to the prototype-to-model length ratio. However, the flexural rigidity scaling factor (λ_{EI}) in Equation (1) was predetermined based on the available instrumented model pile, resulting in a larger effective length scale (λ_L) than the geometric ratio. This effective λ_L was used in Equation (2) to determine the frequency scaling factor (λ_f), ensuring dynamic similarity between model and prototype, while the geometric length of the model pile was retained despite this discrepancy.

Scaling laws are also applied to the input ground motions, ensuring that the model experiences dynamically equivalent excitation. A smooth spectrum method [12] adjusts the peak ground acceleration (PGA) and peak ground velocity (PGV) to retain realistic frequency content. The scaled and unscaled natural frequencies are estimated using Equations (3) and (4):

$$\omega_{nm} = \frac{PGA_{scaled} \cdot \alpha_A}{PGV_{scaled} \cdot \alpha_V} \tag{3}$$

$$\omega_{np} = \frac{PGA_{unscaled} \cdot \alpha_A}{PGV_{unscaled} \cdot \alpha_V} \tag{4}$$

where $\alpha_A = 2.16$ and $\alpha_V = 1.64$ for 5% damping. Consistency between the model and prototype response is confirmed by comparing their scaled frequency ratio with the theoretical ratio in Equation (5):

$$\frac{\omega_{nm}}{\omega_{np}} = \frac{\omega_m}{\omega_p} = \lambda_f \tag{5}$$

This alignment verifies that the essential dynamic characteristics, including the impact of SSI, are preserved in the scaled test. In this study, the calculated frequency scaling factor was found to be $\lambda_f = 27$, confirming consistency between model and prototype response.

The mass of the SDOF oscillator, m_B, is estimated based on the system's natural frequency and stiffness parameters, as shown in Equation (6):

$$m_B = \frac{\left(k_B^{-1} + \hat{k}_{tt}^{-1}\right)^{-1}}{\omega_m^2} \tag{6}$$

where k_B and $\hat{k}_{tt}$ denote the stiffnesses of the superstructure and soil-pile system, respectively. This formulation ensures consistency in inertial interaction, which is critical to accurately capturing SSI effects in the experimental model.

The experimental campaign was conducted at the Earthquake and Large Structures (EQUALS) Laboratory at the University of Bristol. A six-degree-of-freedom shaking table with a 3 m × 3 m platform was used to apply dynamic loading to the model. The soil container was a shear stack originally developed by Dar [13] and later modified by Dietz and Muir Wood [14] to improve flexibility and reduce boundary effects. The box, measuring 1.19 m in length, 0.55 m in width, and 0.814 m in depth, is constructed from alternating aluminium and rubber layers, providing low lateral stiffness. This design enables the soil to dominate the dynamic response, rather than the container. The configuration of the test setup, including the shear box and shaking table arrangement, is illustrated in Figure 1a.

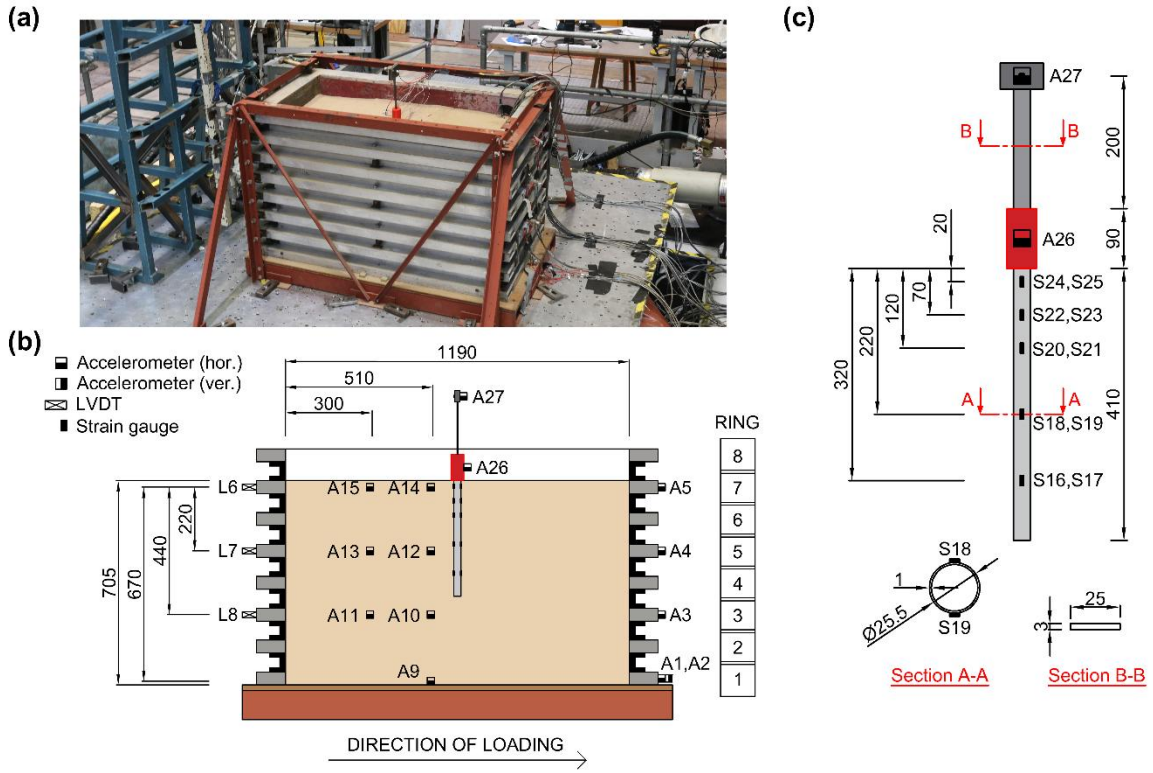

Figure 1: (a) Photograph of the experimental setup; (b) schematic of the shear stack showing instrumentation and dimensions; (c) detail of the single-degree-of-freedom superstructure with monopile, showing sensor locations and dimensions (A: accelerometer; L: LVDT; S: strain gauge). All dimensions in mm.

The sand used in the tests is a fine-grained silica sand known as SoFSI sand. It is light brown in colour, with predominantly subrounded particles. This sand is being extensively used in current studies at the University of Bristol, and its physical and dynamic behaviour under low confinement stress has been characterised in recent work [15, 16].

The instrumentation layout and dimensions are shown in Figures 1b and 1c. Accelerometers placed at the base level along Ring 1 were used to record the input motion. To assess amplification through the soil profile, additional accelerometers and LVDT sensors were installed at three elevations: Rings 3, 4 and 5. At each of these levels, one accelerometer and one LVDT were positioned outside the shear box, while two accelerometers were installed

inside. One was located close to the pile and the other further away, allowing assessment of spatial variation in the soil response.

To capture the dynamic behaviour of the model, two accelerometers were mounted on the structure. One was fixed at the pile cap, representing the pile-to-superstructure connection, and the other was placed on the oscillator mass. These sensors allowed evaluation of the foundation input motion and overall system response.

Strain gauges were used to monitor the bending response of the pile. A total of ten gauges were installed in five opposing pairs along the embedded length. As bending in long piles typically occurs within a limited region near the head, the sensors were concentrated in the upper section. This design is based on the concept of *active pile length* (L_a), which represents the portion of the pile over which significant bending takes place [17, 18]. The active length can be estimated using Equation (7), as proposed by [19]:

$$L_a = \Lambda \left(\frac{E_p}{E_s}\right)^{\mu} d \tag{7}$$

where $\Lambda = 2$ and $\mu = 0.25$ are dimensionless constants suggested by Gazetas [20] for dynamic loading, d is the pile diameter, and E_p and E_s are the Young's moduli of the pile and soil, respectively. Based on these parameters, the active pile length for the test configuration was calculated to be approximately 0.27 m.

To evaluate the natural frequency and damping characteristics of the system, a series of impact tests was conducted. These were performed for both the fixed-base configuration and the soil-structure interaction (SSI) configuration. In the latter case, impact tests were carried out both before and after the application of dynamic excitations to observe any changes in system properties.

In terms of dynamic loading, five scaled ground motion records and a set of white noise tests were applied. A summary of the input motions is provided in Table 2. The earthquake records were originally sourced from the Italian Accelerometric Network (RAN) and were selected from those used in the study by Fiorentino et al. [21].

Input Type	Test ID	Target PGA [g]	Achieved PGA [g]	Moment magnitude, M_w
White noise	WN1	0.06	0.06	–
Seismic record	AMT50	0.09	0.02	5.4
White noise	WN2	0.06	0.06	–
Seismic record	SELE50	0.09	0.09	5.0
White noise	WN3	0.06	0.06	–
Seismic record	CSC100	0.14	0.11	6.5
White noise	WN4	0.06	0.06	–
Seismic record	AMT500	0.34	0.06	6.2
White noise	WN5	0.06	0.06	–
Seismic record	AMT500*	0.70	0.55	6.5
White noise	WN6	0.06	0.06	–

Table 2: Summary of dynamic excitations applied during experimental testing *(Note: AMT500 and AMT500* are distinct ground motion records. The asterisk is used solely for identification purposes).*

Due to the high scaling factor associated with small-scale models, the targeted input motions were not fully achieved. This is primarily because the frequency capacity of the shaking table used in the tests is limited to 50 Hz. Beyond this threshold, the recorded data

becomes dominated by noise, restricting the effective frequency content of the input. The results of both the impact tests and the dynamic excitations are presented in the following section.

3 TEST RESULTS

3.1 Impact test response

Initial impact tests were conducted in both the +y and –y directions to determine the natural frequency and damping ratio of the fixed-base configuration. The average results yielded a natural frequency of 10.0 Hz and a damping ratio of 0.9%, as shown in Figure 2a. To evaluate the dynamic characteristics of the system with soil-structure interaction, impact tests were also performed on the superstructure placed within the soil-filled shear box. Before the application of dynamic excitation, the natural frequency and damping ratio were reduced to 8.4 Hz and 0.7% respectively, as illustrated in Figure 2b. Following excitation, both values showed a slight increase, reaching 8.6 Hz and 1.0% (Figure 2c). A second peak was observed in both cases corresponding to the eigenfrequency of the surrounding elastic soil, which increased marginally from 25.1 Hz to 25.2 Hz. These results reflect the influence of soil-structure interaction on the dynamic response and highlight the need to assess SSI effects in design.

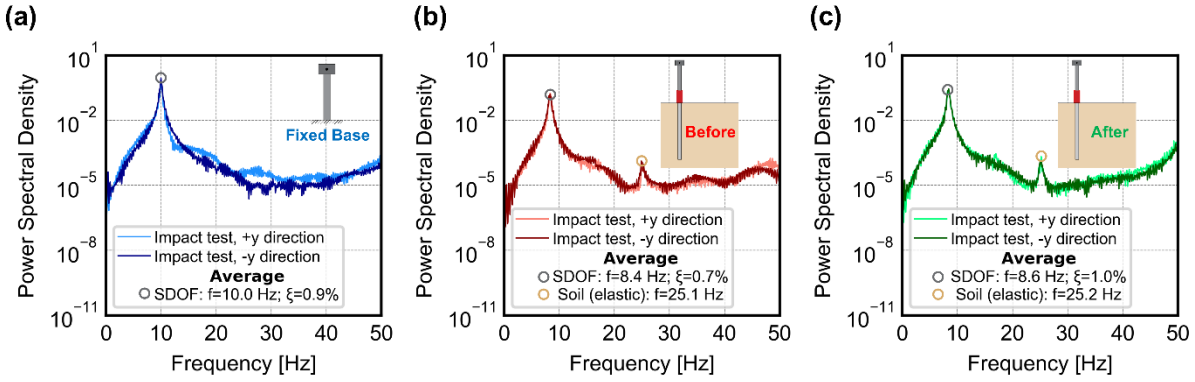

Figure 2: Power spectral density (PSD) of the oscillator mass under: (a) fixed-base condition, flexible-base condition considering pile-soil interaction (b) before and (c) after experimental testing. Impact test results from +y and –y directions and their averaged frequency and damping values are presented.

3.2 Dynamic response

Building on these observations, five scaled ground motion records and a series of white noise inputs were applied. The power spectral densities of the input motions are shown in Figure 3a. Transfer functions were calculated between the acceleration measured at the soil base and that recorded at the oscillator mass, with the resulting changes in frequency and damping ratio presented in Figure 3b. A reduction in natural frequency was observed for all excitation levels when compared to the fixed-base configuration. For example, the lowest-intensity input (AMT50) produced a reduction of fundamental frequency to 9 Hz, while higher-intensity records led to more pronounced decreases, with the frequency dropping to 8.6 Hz and the damping ratio increasing to approximately 2.5%. These results demonstrate the progressive influence of soil-structure interaction with increasing excitation intensity.

To further examine how dynamic excitation influences system behaviour, transfer functions were computed from the soil base to the free-field and from the free-field to the oscillator mass. The response to the lowest-intensity input motion (AMT50) is illustrated in Figures 4a and 4b. The Fourier amplitude spectrum is shown in Figure 4a, and the corresponding transfer functions are presented in Figure 4b. Under this excitation, the eigenfrequency of the soil increased to

39.3 Hz relative to the baseline elastic condition, indicating a stiffer response at lower excitation levels. In contrast, for the highest-intensity input motion (AMT500*), the soil eigenfrequency decreased significantly to 15.4 Hz (Figures 4c and 4d), reflecting a reduction in stiffness attributed to nonlinear soil behaviour. Notably, under strong excitation, the soil frequency shifts closer to the natural frequency of the superstructure, suggesting increased potential for resonance and enhanced dynamic interaction. These findings reinforce the importance of capturing nonlinear soil behaviour when assessing SSI effects under varying levels of seismic loading.

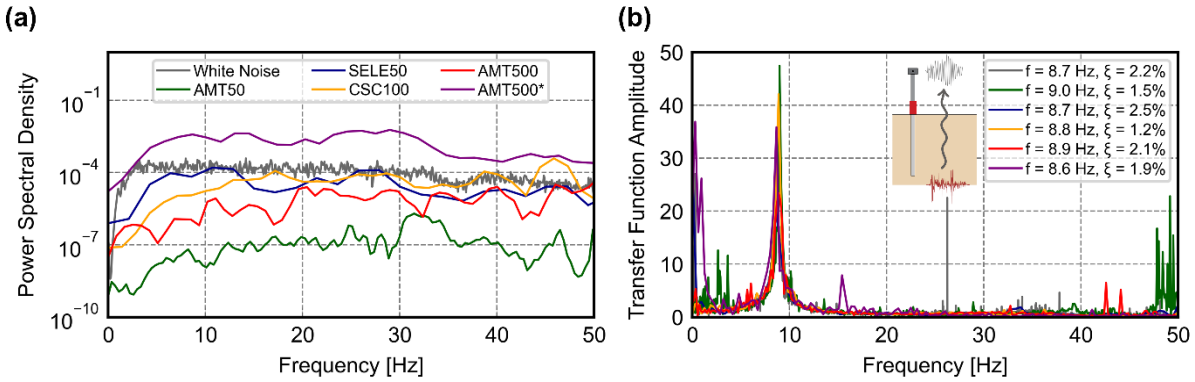

Figure 3: (a) Power spectral density of input motions; (b) Transfer functions from the soil base to the oscillator mass, indicating corresponding natural frequencies and damping ratios for each input motion.

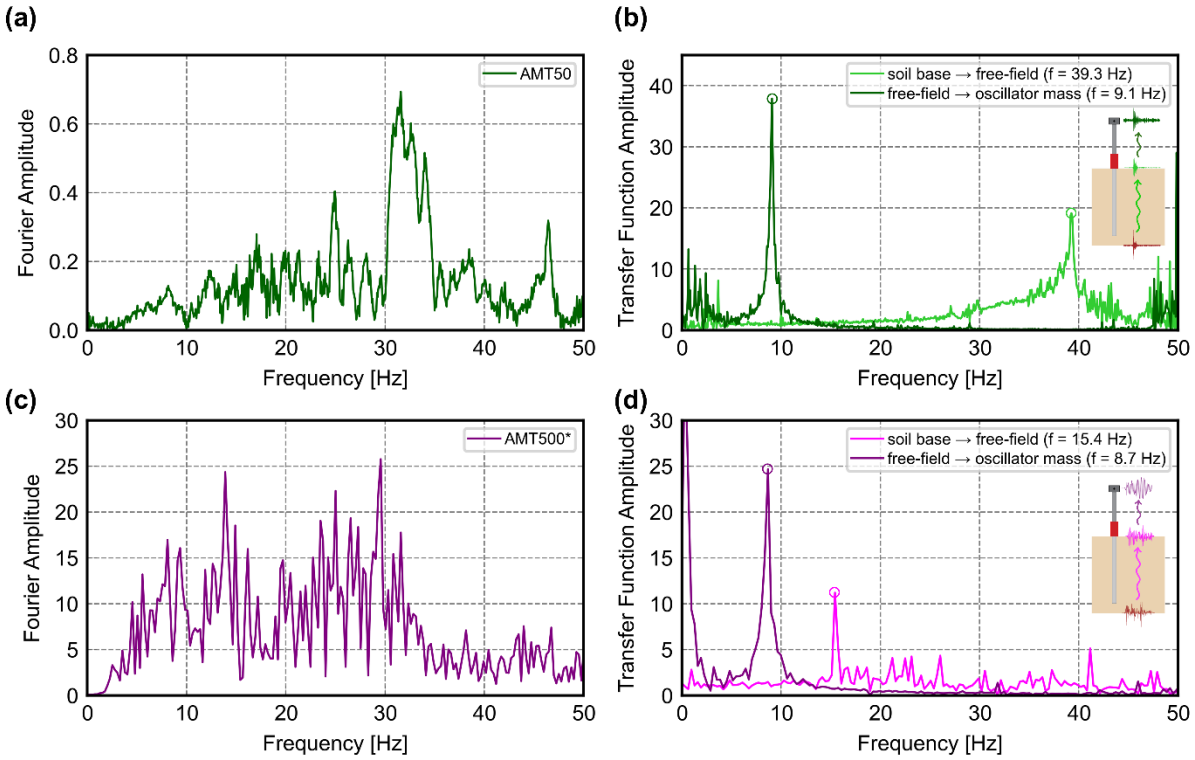

Figure 4: Fourier amplitude spectra of the lowest (a) and highest (c) intensity input motions (AMT50 and AMT500*, respectively), and corresponding transfer functions (b, d) from the soil base to the free-field and from the free-field to the oscillator mass. Natural frequencies associated with each input are indicated in the transfer function plots.

3.3 Bending strain response

The strain response was recorded for each input motion. Bending strain was calculated from the difference between strain measurements on opposing sides of the pile, assuming one side is in tension and the other in compression. The resulting bending strain was then divided by the gauge spacing, which corresponds to the outer diameter of the pile (25.5 mm), to determine the curvature. This curvature was multiplied by the flexural rigidity of the pile to calculate the bending moment, as shown in Figure 5.

The absolute maximum bending moment was consistently observed near the pile head, at the location of strain gauges S24 and S25 (see Figure 1). The bending moments at the remaining four levels were extracted at the corresponding time instant and are included in the diagrams for comparison. As illustrated in Figure 5, the bending moment at high excitation levels (e.g. AMT500*) reached approximately 4 N·m, while for low-intensity input motions (e.g. AMT50), it remained below 0.1 N·m near the pile head, where maximum deflection occurs. These results confirm that under low excitation levels, the system exhibits predominantly elastic behaviour, whereas under strong input motions, nonlinear soil response becomes the dominant factor controlling system behaviour.

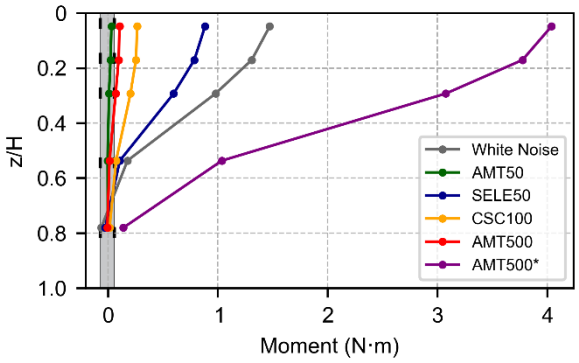

Figure 5: Bending moment diagrams derived from experimental measurements for each input motion.

4 EXPERIMENTAL-TO-ANALYTICAL COMPARISONS

An analytical estimate of the natural frequency for the fixed-base configuration was calculated using the flexural rigidity of the steel bar (11.25 N·m²) and an oscillator mass of approximately 1 kg. This yielded a frequency of 10.3 Hz, which is in close agreement with the experimentally observed value of 10.0 Hz. The minor difference may be attributed to modelling assumptions, such as the use of an idealised Young's modulus of 200 GPa for the steel.

The response of the pile-soil system was also analysed using the classical *Beam-on-Winkler Foundation (BWF)* model, widely adopted for linear-elastic soil-structure interaction problems in homogeneous soils [22–25]. The governing differential equation for the transverse displacement $y(z)$ of the pile is expressed in Equation (8):

$$y^{(4)}(z) + 4\lambda^4 y(z) = 0 \tag{8}$$

where $y(z)$ is the lateral displacement at depth z, with $z = 0$ at the pile head. The Winkler parameter λ is defined as $\lambda = \left(k/4E_pI\right)^{1/4}$, where k is the modulus of the subgrade reaction, and E_p and I are the Young's modulus and second moment of area of the pile, respectively.

The general solution to Equation (8) is given in Equation (9):

$$y(z) = C_1 e^{-\lambda z}\sin(\lambda z) + C_2 e^{-\lambda z}\cos(\lambda z) \tag{9}$$

The constants C_1 and C_2 are derived from boundary conditions, specifically the pile head displacement y_0 and rotation θ_0. These can be calculated using the stiffness matrix method, as shown in Equation (10):

$$\begin{bmatrix} y_0 \\ \theta_0 \end{bmatrix} = [K]^{-1} \begin{bmatrix} P_0 \\ M_0 \end{bmatrix} \tag{10}$$

where $P_0 = m_B \ddot{u}_B$ is the shear force and $M_0 = P_0 H_B$ is the bending moment applied at the pile head due to the inertial action of the superstructure, with m_B as the oscillator mass, $\ddot{u}_B$ the measured acceleration, and H_B the height of the oscillator.

The stiffness matrix $[K]$ for a free-head pile in a homogeneous elastic soil is provided in Equation (11), based on formulations by Mylonakis [26] and Mylonakis and Gazetas [27]:

$$[K] = \begin{bmatrix} k_{tt} & k_{t\theta} \\ k_{\theta t} & k_{\theta\theta} \end{bmatrix} = \begin{bmatrix} 4E_p I\lambda^3 \frac{\sin(2\lambda L)+\sinh(2\lambda L)}{2+\cos(2\lambda L)+\cosh(2\lambda L)} & 2E_p I\lambda^2 \frac{-\cos(2\lambda L)+\cosh(2\lambda L)}{2+\cos(2\lambda L)+\cosh(2\lambda L)} \\ \text{sym.} & 2E_p I\lambda \frac{-\sin(2\lambda L)+\sinh(2\lambda L)}{2+\cos(2\lambda L)+\cosh(2\lambda L)} \end{bmatrix} \tag{11}$$

where L is the pile length, and the coefficients are expressed as trigonometric and hyperbolic functions of dimensionless parameter λL [28].

To evaluate the modulus of subgrade reaction k, the analytical expression proposed by Karatzia and Mylonakis [29], building on Mylonakis [30], is adopted. This is given in Equation (12):

$$k = \frac{4\pi G \eta_u^2}{(1+\eta_u^2)\left[\ln\left(\frac{4}{\alpha_c}\right)-\gamma\right]+\ln(\eta_u)} \tag{12}$$

where G is the shear modulus of the soil, $\gamma = 0.577$ is the Euler-Mascheroni constant, and η_u is a dimensionless parameter related to Poisson's ratio ν, defined in Equation (13):

$$\eta_u^2 = \frac{2-\nu}{1-\nu} \tag{13}$$

The normalised stiffness parameter is given in Equation (14):

$$\alpha_c = x_\delta \left(\frac{E_p}{E_{s,D}}\right)^{n_\delta} \tag{14}$$

where E_p is the Young's modulus of the pile, $E_{s,D}$ is the soil Young's modulus at a depth equal to one pile diameter, and $x_\delta = 2.125$, $n_\delta = -0.25$ are empirical constants valid for free-head piles in homogeneous soil [29].

To account for only translational stiffness at the pile head, static condensation is applied to reduce the matrix, as shown in Equation (15):

$$\hat{k}_{tt} = k_{tt} - k_{\theta t}^T k_{\theta\theta}^{-1} k_{\theta t} \tag{15}$$

This condensed stiffness is used to estimate the eigenfrequency of the system, including soil flexibility, as presented in Equation (16):

$$\omega_{SSI} = \left[\left(\hat{k}_{tt}^{-1} + k_B^{-1}\right)^{-1} / m_B\right]^{1/2} \tag{16}$$

The resulting frequency is approximately 10.0 Hz, which is higher than the experimentally observed value of around 8.5 Hz. This overestimation is attributed to the use of a linear-elastic model, which does not fully capture the nonlinear soil response observed during testing.

To evaluate the bending strain response, the curvature $\phi(z)$ was calculated as the second derivative of deflection, $y''(z)$, obtained from the BWF model. The corresponding bending moment was then determined by multiplying the curvature with the flexural rigidity E_pI.

Figure 6 presents a comparison between the analytically calculated and experimentally measured bending moments for each input motion. Under low excitation levels (e.g. AMT50), where soil behaviour is predominantly elastic, the analytical model showed close agreement with experimental results. At higher intensities, the model underestimates the response, likely due to nonlinear soil effects and the exclusion of kinematic interaction. The active pile length predicted by the model corresponds to approximately mid-depth ($z/H \approx 0.5$), consistent with the location of observed peak bending moments.

While the simplified model offers reliable estimates under elastic conditions, these results highlight the importance of incorporating nonlinear soil behaviour and complete SSI mechanisms in future analytical formulations. This reinforces the value of integrated experimental-analytical approaches in improving the design and assessment of monopile-supported offshore wind turbines.

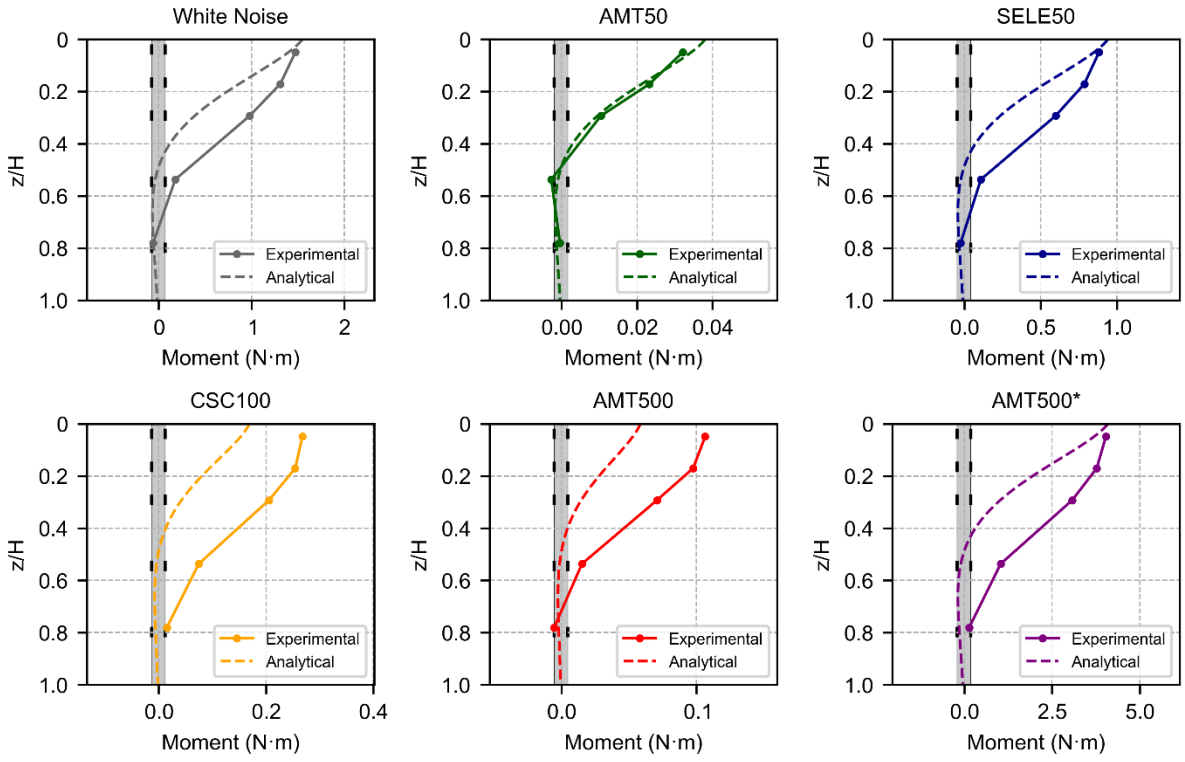

Figure 6: Comparison of bending moment distributions from experimental measurements and analytical predictions for each input motion. Depth is expressed as a normalised ratio (z/H), where z is the pile depth and H is the total pile length.

CONCLUSIONS

Based on the integrated experimental and analytical investigation of soil-structure interaction (SSI) effects in a monopile-supported wind turbine model, the following conclusions can be drawn:

- SSI significantly influences the dynamic characteristics of the structure, leading to reductions in natural frequency and increases in damping. These effects become more

pronounced with increasing excitation intensity, demonstrating the progressive nature of soil nonlinearity in dynamic response.

- Experimental results confirm that the system behaviour is largely elastic at low input levels, while higher-intensity motions induce nonlinear soil response. This transition has a clear influence on both energy dissipation and the distribution of internal forces, particularly in the embedded portion of the pile.
- The Beam-on-Winkler analytical model, based on linear-elastic assumptions, provides good agreement with experimental bending moments under weak excitations. However, it consistently underestimates the response under strong ground motions. This outcome reflects the model's limitations in capturing strain-dependent stiffness degradation and hysteretic damping, as well as its exclusion of kinematic interaction effects.
- The active pile length observed experimentally corresponds well with theoretical estimates, confirming the validity of simplified assumptions regarding the effective embedded depth contributing to bending resistance in monopiles.
- The study demonstrates the value of integrating small-scale testing with analytical formulations, providing a robust framework for validating dynamic SSI models in wind turbine applications. The results highlight important physical trends that can inform the calibration of more advanced nonlinear numerical tools.
- While the present study adopts a linear-elastic soil model for analytical comparison and relies on a relatively high scaling factor, the findings offer meaningful insights for prototype-scale behaviour and can guide more comprehensive SSI investigations.

Future studies should incorporate calibrated numerical models. For example, finite element analyses using nonlinear soil constitutive laws and complete soil-pile interaction formulations could be employed to more accurately predict system behaviour under strong dynamic loading. These developments will help enhance the reliability of SSI-inclusive design methods for offshore wind turbines.

ACKNOWLEDGEMENTS

Shahin Huseynli gratefully acknowledges the support provided by the "State Programme 2019-2023" of the Ministry of Science and Education of the Republic of Azerbaijan. The authors also extend their sincere thanks to the technical team at the Earthquake and Large Structures (EQUALS) Laboratory at the University of Bristol for their assistance throughout the experimental campaign. In particular, they wish to acknowledge Mr David Williams (Laboratory Manager), Mr Mictroy Mitchell, and Mr Jake Limer for their valuable support during the preparation and execution of the tests.

REFERENCES

[1] D. Lombardi, S. Bhattacharya, D.M. Wood, Dynamic soil-structure interaction of monopile supported wind turbines in cohesive soil. *Soil Dynamics and Earthquake Engineering*, **49**, 165–180, 2013.

[2] S. Bhattacharya, S. Adhikari, Experimental validation of soil-structure interaction of offshore wind turbines. *Soil Dynamics and Earthquake Engineering*, **31**(5–6), 805–816, 2011.

[3] K. Lin, B. Ma, S. Yang, A. Zhou, Experimental study of wind turbine in operation under wind and seismic excitations with soil-structure interaction. *Engineering Structures*, **308**, 117927, 2024.

[4] M. Shahidikhah, M. Moradi, B. Gatmiri, 1 g shaking table test for seismic response for a monopile foundation of offshore wind turbine. *Applied Ocean Research*, **150**, 104096, 2024.

[5] M. Shahidikhah, M. Moradi, A. Bateni, A. Ghalandarzadeh, Assessing the effect of monopile dimensions on seismic response of offshore wind turbines. *Ocean Engineering*, **317**, 120090, 2025.

[6] L. Arany, S. Bhattacharya, J.H. Macdonald, S.J. Hogan, Closed form solution of Eigen frequency of monopile supported offshore wind turbines in deeper waters incorporating stiffness of substructure and SSI. *Soil Dynamics and Earthquake Engineering*, **83**, 18–32, 2016.

[7] Z. Zhang, R. De Risi, A. Sextos, Multi-hazard fragility assessment of monopile offshore wind turbines under earthquake, wind and wave loads. *Earthquake Engineering & Structural Dynamics*, **52**(9), 2658–2681, 2023.

[8] W. He, A. Takahashi, Dynamic response analysis of monopile-supported offshore wind turbine on sandy ground under seismic and environmental loads. *Soil Dynamics and Earthquake Engineering*, **189**, 109105, 2025.

[9] L.V. Andersen, M.J. Vahdatirad, M.T. Sichani, J.D. Sørensen, Natural frequencies of wind turbines on monopile foundations in clayey soils—A probabilistic approach. *Computers and Geotechnics*, **43**, 1–11, 2012.

[10] A. Ali, R. De Risi, A. Sextos, K. Goda, Z. Chang, Seismic vulnerability of offshore wind turbines to pulse and non-pulse records. *Earthquake Engineering & Structural Dynamics*, **49**(1), 24–50, 2020.

[11] D. Muir Wood, *Geotechnical Modelling*. CRC Press, 2004.

[12] P.K. Malhotra, Smooth spectra of horizontal and vertical ground motions. *Bulletin of the Seismological Society of America*, **96**(2), 506–518, 2006.

[13] A.R. Dar, *Development of a flexible shear stack for shaking table testing of geotechnical problems*. PhD Thesis, University of Bristol, UK, 1993.

[14] M. Dietz, D. Muir Wood, Shaking table evaluation of dynamic soil properties. In *Proceedings of the 4th International Conference on Earthquake Geotechnical Engineering*, Thessaloniki, Greece, June 25–28, 2007.

[15] Z. Huang, *Soil test report for SoFSI sand*. Unpublished research report, University of Bristol, UK, 2023.

[16] S. Huseynli, E.E. Lee, D. Karamitros, M.S. Dietz, F. De Luca, Dynamic characterization of sand under low confinement stress via shear box testing on shaking table. *Soil Dynamics and Earthquake Engineering*, **195**, 109398, 2025.

[17] R. Di Laora, E. Rovithis, Kinematic bending of fixed-head piles in nonhomogeneous soil. *Journal of Geotechnical and Geoenvironmental Engineering*, **141**(4), 04014126, 2015.

[18] X. Karatzia, G. Mylonakis, Discussion of "Kinematic bending of fixed-head piles in nonhomogeneous soil" by Raffaele Di Laora and Emmanouil Rovithis. *Journal of Geotechnical and Geoenvironmental Engineering*, **142**(2), 07015042, 2016.

[19] NIST, *Soil-structure interaction for building structures*. NIST GCR 12-917-21, NEHRP Consultants Joint Venture, Maryland, 2012.

[20] Gazetas, Foundation vibrations. In: H.-Y. Fang (ed.), *Foundation Engineering Handbook*, 2nd Edition, Chapter 15, Chapman and Hall, New York, 1991.

[21] G. Fiorentino, C. Cengiz, F. De Luca, G. Mylonakis, D. Karamitros, M. Dietz, L. Dihoru, D. Lavorato, B. Briseghella, T. Isakovic, C. Vrettos, Integral abutment bridges: investigation of seismic soil-structure interaction effects by shaking table testing. *Earthquake Engineering & Structural Dynamics*, **50**(6), 1517–1538, 2021.

[22] M.A. Biot, Bending of an infinite beam on an elastic foundation. *Journal of Applied Mechanics ASME*, **4**(1), A1–A7, 1937.

[23] M. Hetényi, *Beams on Elastic Foundation*. The University of Michigan Press, Ann Arbor, MI, USA, 1946.

[24] H.G. Poulos, E.H. Davis, *Pile Foundation Analysis and Design*. Wiley, New York, NY, USA, 1980.

[25] R.F. Scott, *Foundation Analysis*. Prentice Hall, Englewood Cliffs, NJ, USA, 1981.

[26] G. Mylonakis, *Contributions to static and seismic analysis of piles and pile-supported bridge piers*. PhD Thesis, State University of New York at Buffalo, Buffalo, NY, USA, 1995.

[27] G. Mylonakis, G. Gazetas, Lateral vibration and internal forces of grouped piles in layered soil. *Journal of Geotechnical and Geoenvironmental Engineering*, **125**(1), 16–25, 1999.

[28] G.E. Mylonakis, J.J. Crispin, Simplified models for lateral static and dynamic analysis of pile foundations. In: *Analysis of Pile Foundations Subject to Static and Dynamic Loading*, CRC Press, 185–245, 2021.

[29] X. Karatzia, G. Mylonakis, Horizontal stiffness and damping of piles in inhomogeneous soil. *Journal of Geotechnical and Geoenvironmental Engineering*, **143**(4), 04016113, 2017.

[30] G. Mylonakis, Elastodynamic model for large-diameter end-bearing shafts. *Soils and Foundations*, **41**(3), 31–44, 2001.